Journal of ELECTRONIC MATERIALS, Vol. 46, No. 10, 2017
DOI: 10.1007/s11664-017-5570-1

Enhanced Luminescence of La^{3+}-Doped Gadolinium Oxysulfide with Tunable Crystalline Size

YU-JIE DING,[1,2] LI-XI WANG,[1,2] QI-TU ZHANG,[1,2,4] and SHI-BING PAN[3]

1.—College of Materials Science and Engineering, Nanjing Tech University, No. 5 Xin Mofan Road, Gulou District, Nanjing 210009, China. 2.—Jiangsu Collaborative Innovation Center for Advanced Inorganic Function Composites, No. 5 Xin Mofan Road, Gulou District, Nanjing 210009, China. 3.—Institute 53 of China's Ordnance Industry, No. 3 Tian Jiazhuang East Road, Tianqiao District, Jinan 250000, China. 4.—e-mail: ngdzqt@163.com

The concentration of La^{3+} in $(La_xGd_{1-x})_2O_2S$:Tb phosphors prepared by the sulfide fusion method from coprecipitated oxalate precursors has been tuned, and the prominent effect on the crystalline size, particle size, and luminescence properties investigated. First-principles calculations were used to characterize the charge deformation, energy gap, and crystal field. According to density functional theory, the electron density of states in conduction bands increased with increase in the La^{3+} concentration. The increased electronic density strengthened the repulsion and thus decreased the diffusion so as to decrease the crystalline size from 106.2 nm to 37.3 nm. The particle size of $(La_xGd_{1-x})_2O_2S$:Tb increased from 0.21 μm to 1.25 μm as the La^{3+} concentration was increased from 15 mol.% to 60 mol.%. The excitation spectrum shifted towards shorter wavelength, enhancing the luminescence intensity of $(La_xGd_{1-x})_2O_2S$:Tb when excited at 254 nm. Furthermore, shorter lifetime was obtained due to lower symmetry as more Gd^{3+} was substituted by La^{3+} ions.

Key words: Phosphors, first-principles calculations, luminescence, lifetime, symmetry

INTRODUCTION

Rare-earth doping is an intriguing method, since such intentional introduction can selectively tailor the properties of the doped material. Incorporating trivalent rare-earth ions into the host lattice has frequently been adopted as it can yield hybrid materials with desirable properties and functions. Previous studies have reported that Tb^{3+} can efficiently generate bright-green light when doped into appropriate substrates.[1–3] Tb^{3+}-activated oxysulfides have attracted great interest for use in ultraviolet (UV) imaging systems.[4,5] Most such phosphors for this application are characterized at 254 nm.[6] Oxysulfides (Ln_2O_2S; Ln = La, Gd, Y) are considered as ideal host materials because of their low phonon energy, nontoxicity, and low symmetry,[7,8] among which Ln_2O_2S is considered to be one of the most effective for use in fluorescence applications.[4] Current applications of Ln_2O_2S phosphors include televisions,[9] catalysts,[10] upconversion lasers,[11] scintillation materials,[12] etc. Especially for application in display devices, smaller particles with high luminescence intensity are used to improve resolution.[13]

Therefore, rare-earth dopants are expected not only to introduce novel properties, but also to affect the particle size, phase, and emission intensity of Ln_2O_2S phosphors.[14] Wang et al.[15] demonstrated that addition of Gd^{3+} could control the size, phase, and upconversion emission of $NaYF_4$. Similarly, Chen et al.[16] reported that lanthanide doping of an alkaline-earth metal fluoride resulted in significantly improved monodispersity. A common strategy for enhancing the luminescence is to tune the doping concentration of lanthanide ions,[17,18] but high doping level may lead to concentration

(Received November 25, 2016; accepted May 2, 2017; published online May 15, 2017)

quenching, particularly in the short-wavelength spectral region, which may deteriorate the luminescence intensity. Also, energy transfer from the host or sensitizer to an activator in many inorganic hosts has been demonstrated to be effective to improve the luminescence intensity.[5]

Although use of Gd_2O_2S as single-phase substrate material has been reported in many papers, few of them studied the Gd–La binary oxysulfide system. As a host material for Tb^{3+}, we focus here on incorporation of La^{3+} into Gd_2O_2S:Tb to form a La–Gd oxysulfide solid solution. All samples were prepared using the sulfide fusion method. Particle sizes ranging from 0.21 μm to 1.25 μm were achieved by tuning the La^{3+} concentration in the La–Gd oxysulfides. Furthermore, the luminescence intensity could be enhanced by elevating the concentration of La^{3+}.

EXPERIMENTAL PROCEDURES

Materials

Rare-earth oxides RE_2O_3 (RE = Gd, La) and Tb_4O_7 (99.99%, Liyang Luodiya Rare Earth New Materials Co., Ltd.) were used as starting materials. Na_2CO_3 and S (Sinopharm Group Co. Ltd.) were used as fluxes. All regents were of analytical grade and used directly without any further purification.

Methods

$(La_xGd_{1-x})_2O_2S$:Tb (Gd-La:Tb) particles were prepared as follows: Gd_2O_3 and La_2O_3 were weighed precisely according to stoichiometric ratio. The obtained powder mixture was dissolved in HNO_3 at elevated temperature, then oxalate precursors were prepared by coprecipitation using oxalic acid as precipitator. $(Gd_{1-x}La_x)_2O_3$ powders were obtained by calcination of the precursors at 1000°C. The mixed powders of $(Gd_{1-x}La_x)_2O_3$, Tb_4O_7, Na_2CO_3, and S were then ball milled at molar ratio of 1:0.02:1.5:4. After compaction, the mixed bulk was wrapped in a double-jacketed alumina crucible, while Al_2O_3 powder was filled into the interstice between the two crucibles. Synthesis was then performed at 1100°C for 3 h in an electric furnace with heating rate of 5°C/min. Finally, the calcined products were washed several times with deionized water and alcohol to remove possible byproducts from the preparation process, and subsequently dried at 80°C to obtain the prepared phosphors.

Characterization

The phase composition of the samples was identified by x-ray diffraction (XRD, Shimadzu XRD-6000) analysis using Cu $K_{\alpha 1}$ radiation. For consistency, the XRD patterns of the Gd-La:Tb samples were obtained on the same day, and a silicon standard was used as control to ensure repeatability. The particle size and morphology of the phosphors were observed by field-emission scanning electron microscopy (FE-SEM, Hitachi S-4800). Diffuse reflectance spectra were recorded in the region from 200 cm^{-1} to 700 cm^{-1} using an ultraviolet–visible light detector (UV-3600PC, Shimadzu, Japan). The luminescence properties of the oxysulfide phosphors were analyzed using a fluorescence spectrophotometer (Lumina) at 500 V with a 1 nm/1 nm slit, and fluorescence decay curves were obtained using a fluorescence spectrometer (FLsp9, UK). The density of states (DOS), partial density of states (PDOS), and electronic band structure (EBS) were calculated based on density functional theory (DFT), optimizing the geometry of the crystal structures using the generalized gradient approximation. The specific surface area and pore size were obtained using a physisorption analyzer (ASAP 2020, Micromeritics) at condition of −196.15°C.

RESULTS AND DISCUSSION

Phase and Crystalline Size

The doping concentrations of La^{3+} in the phosphors were 0 mol.%, 15 mol.%, 30 mol.%, 45 mol.%, and 60 mol.%, while the molar ratio of Tb^{3+} was fixed at 2 mol.%. For all samples, bright-green light could be seen by the naked eye under 254-nm UV lamp illumination (Supplementary Fig. 1). Figure 1a shows the XRD pattern of the Gd_2O_2S:Tb (GOST) phosphor. As can be seen from Fig. 1a, GOST presented typical hexagonal structure according to Joint Committee on Powder Diffraction Standards (JCPDS) card no. 26-1422. Addition of Tb^{3+} did not change the inherent crystal structure of Gd_2O_2S. Figure 1b shows the emission spectrum of GOST when excited at 254 nm, revealing the highest-intensity peak at 544 nm. Figure 1c and d depict the morphology and particle distribution of GOST; the average particle size of GOST was 1 μm to 2 μm.

Figure 2 shows the characteristic XRD peaks of the Gd-La:Tb phosphors as a function of the La^{3+} concentration. The diffraction peaks of the Gd-La:Tb phosphors shifted towards lower diffraction angle as the La^{3+} doping concentration was increased, indicating expansion of the unit cell (as shown in Supplementary Table 1). This expansion phenomenon is attributed to substitution of Gd^{3+} by larger La^{3+} ions in the host lattice. According to the Scherrer equation,[19] the average crystalline size was calculated based on the XRD patterns (Table I), decreasing from 106.2 nm to 37.3 nm with increasing La^{3+} concentration. The calculated crystalline size of Gd_2O_2S:Tb is similar to that reported by Yan.[20]

The ionic radius of Gd^{3+} (r = 0.0938 nm) is smaller than that of La^{3+} (r = 0.1032 nm). Lattice distortion occurs when Gd^{3+} is replaced with La^{3+} ion in the crystal lattice, and the electron charge density thus increases. Figure 3a presents the isosurface of electronic density, while Fig. 3b shows the repulsion of negative atoms due to the increased

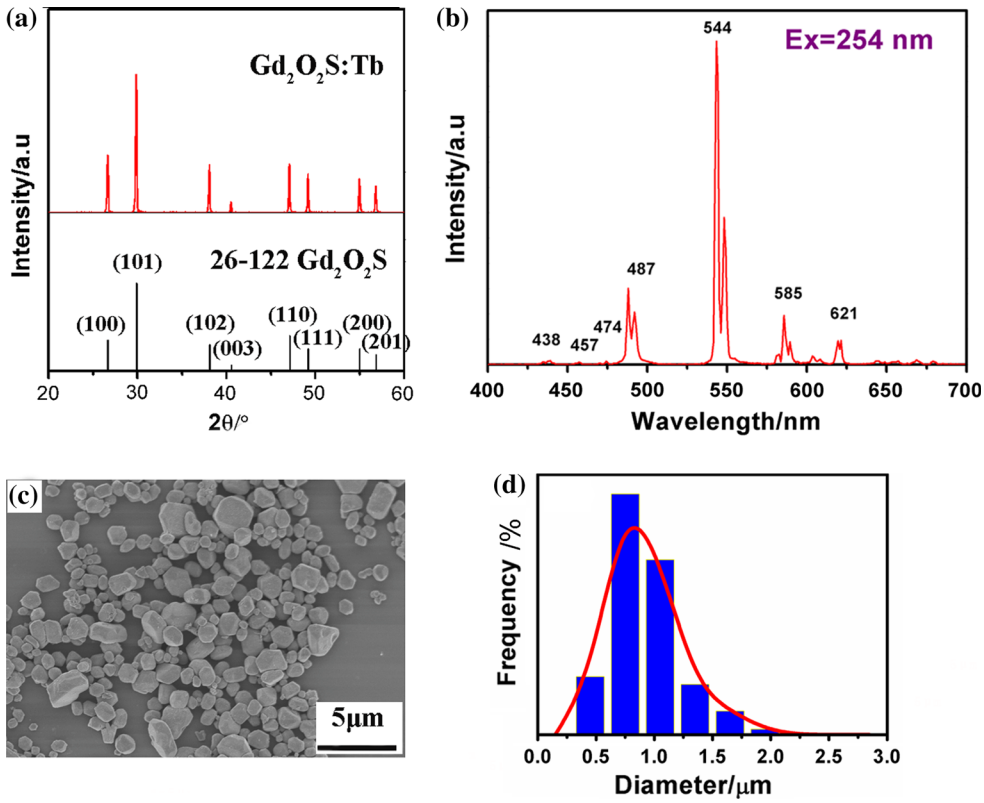

Fig. 1. (a) X-ray powder diffraction pattern, (b) emission spectrum, (c) SEM image, and (d) particle size distribution of Gd_2O_2S:Tb.

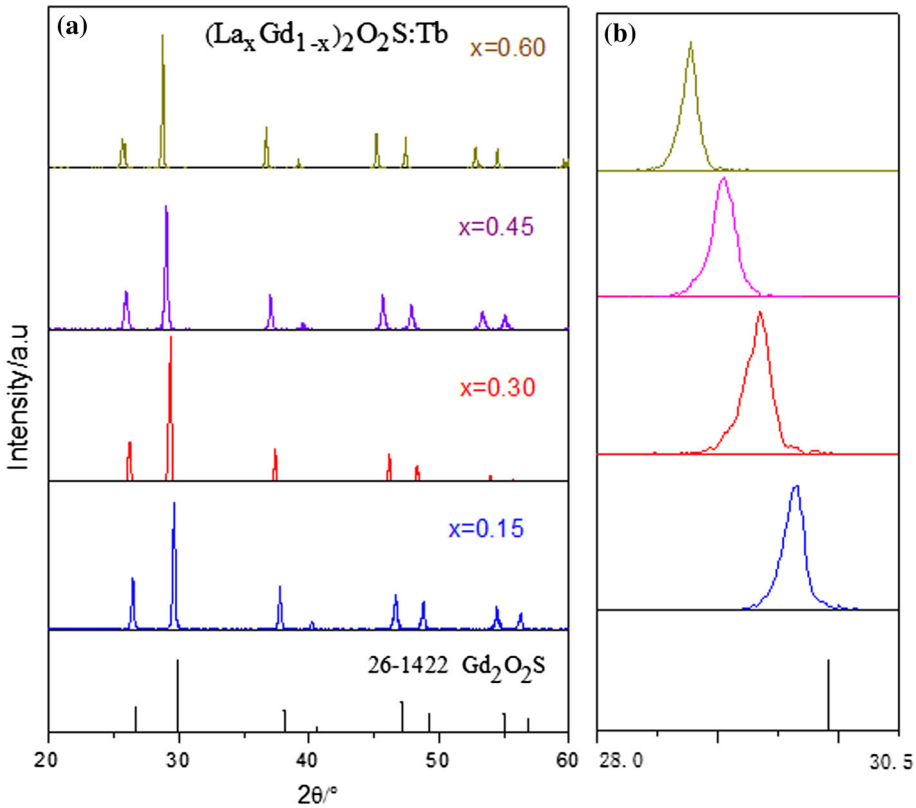

Fig. 2. (a) X-ray powder diffraction patterns of Gd-La:Tb (x = 0.15, 0.3, 0.45, 0.6), and (b) the gradual shift towards lower angle with increasing amount of La^{3+}.

Table I. Average particle size and calculated crystalline size of Gd-La:Tb phosphors

Sample	Average particle size (μm)	Calculated crystalline size (nm)
Gd_2O_2S:Tb	1.14	106.2
$(La_{0.15}Gd_{0.85})O_2S$:Tb	0.21	88.9
$(La_{0.30}Gd_{0.70})O_2S$:Tb	0.24	50.3
$(La_{0.45}Gd_{0.55})O_2S$:Tb	0.8	48.5
$(La_{0.60}\ Gd_{0.40})O_2S$:Tb	1.25	37.3

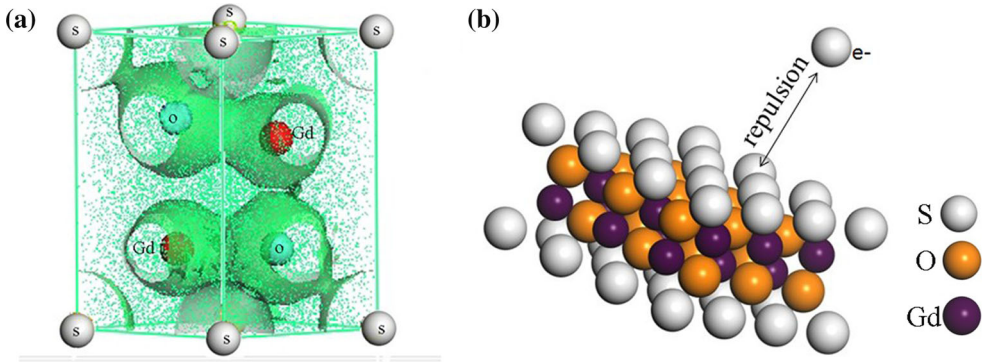

Fig. 3. (a) Isosurface of electronic density. (b) Schematic illustration of repulsion of negative atoms.

surface electron density. The enhanced charge repulsion is caused by the increased electron charge density on the surface, retarding diffusion of negative ions to the surface and thus leading to the reduced crystalline size of the Gd-La:Tb phosphors.[15]

To gain insight into the size control mechanism, Fig. 4 presents the electronic band structure (EBS), density of states (DOS), and partial density of states (PDOS) of the oxysulfide phosphors. The bandgap of Gd_2O_2S, $(La_{0.15}Gd_{0.85})_2O_2S$, and $(La_{0.6}Gd_{0.4})_2O_2S$ was approximately 4.22 eV, 3.82 eV, and 3.52 eV, respectively. The PDOSs show that the top edge of the valence band mainly consisted of O 2*p* and S 2*p* orbitals, while the conduction bands mainly consisted of Gd 5*d* and La 5*d* orbitals. In contrast to GOST, the density of states of conduction bands increased intensively when Gd^{3+} was substituted by increasing amounts of La^{3+}. This increasing density of states strengthens the electron charge density on the surface, thereby increasing the charge repulsion. Moreover, expansion of the conduction band width narrows the energy gap. Consequently, narrower energy gap corresponds to higher electron density.

Mott–Davis theory was applied to calculate the energy gap of Gd-La:Tb.[21,22] For an indirect-bandgap semiconductor such as La_2O_2S[23] and Gd_2O_2S,[24] the bandgap energy can be obtained from the following equation:

$$\alpha h\upsilon = C \times (h\upsilon - E_{\text{opt}})^2, \quad (1)$$

where α is the absorption coefficient, E_{opt} is the bandgap energy, C is a constant, and $h\upsilon$ is the photon energy. Curves of $\alpha h\upsilon$ versus $h\upsilon$ were constructed as shown in Fig. 5. As more Gd^{3+} was substituted by La^{3+}, the energy gap decreased from 4.13 eV to 3.48 eV, in accordance with the results calculated based on DFT. Due to the Tb^{3+} doping, the energy gaps calculated based on DFT are higher than those based on Mott–Davis theory. It is important to note that the decreased energy gaps are well consistent with the reduced crystalline sizes (Table I).

Dependence of Particle Size on La^{3+} Doping

The La^{3+} doping level had a significant impact on the morphology of the Gd-La:Tb phosphors. Figure 6 presents FE-SEM images and the particle size distributions of Gd-La:Tb. The mean particle sizes are summarized in Table I. Compared with GOST, there was a sharp decrease in particle size when 15 mol.% La^{3+} was doped into GOST. The size of the microparticles increased from 0.21 μm to 1.25 μm as the La^{3+} doping was increased from 15 mol.% to 60 mol.%.

The as-prepared $(Gd_{1-x}La_x)_2O_3$ used to prepare the phosphors is also important to the morphology of the resulting Gd-La:Tb. Figure 7 shows the nitrogen adsorption–desorption isotherms and corresponding pore size distributions for Gd_2O_3 and $(La_{0.15}Gd_{0.85})_2O_3$. The specific surface area of the particles was measured by the Brunauer–Emmett–Teller (BET) method, while the pore size was computed using the Barrett–Joyner–Halenda (BJH) method. The surface area of Gd_2O_3 was found

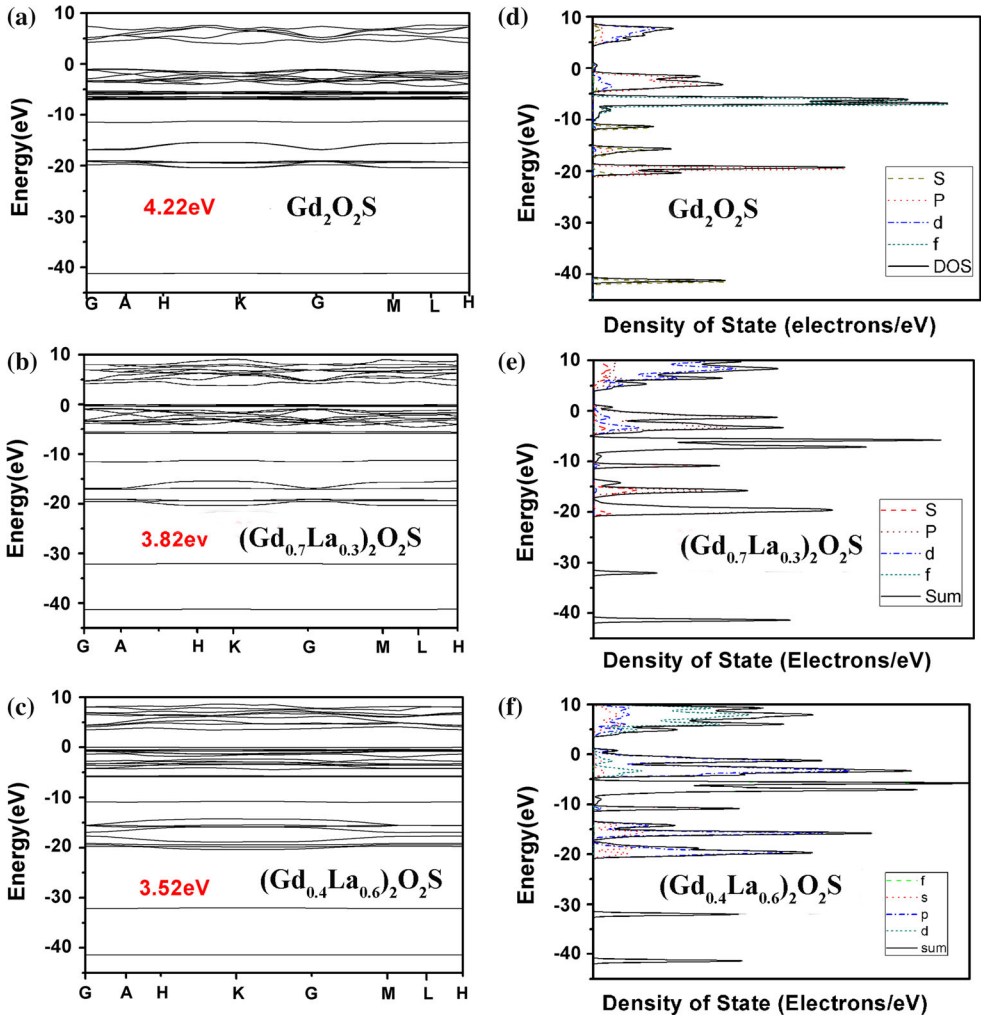

Fig. 4. Electronic band structure (a–c) and density of states and partial densities of state (d–f) for: (a, d) Gd_2O_2S, (b, e) $(La_{0.3}Gd_{0.7})_2O_2S$, and (c, f) $(La_{0.6}Gd_{0.4})_2O_2S$.

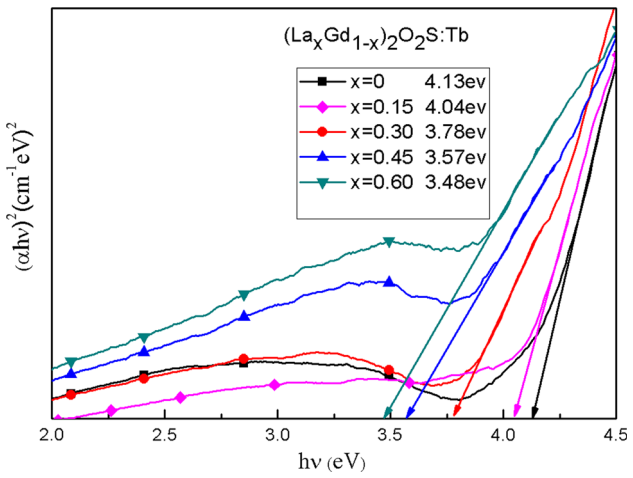

Fig. 5. Energy gaps of Gd-La:Tb calculated by Mott–Davis theory.

to be 8.117 m^2/g, higher than that of $(La_{0.15}Gd_{0.75})_2O_3$ (0.988 m^2/g). The surface area, average pore size, and pore volume were calculated and are presented in Table II. Both isotherms are of type III, with hysteresis loops occurring due to capillary condensation from pores. Mesoporous materials with larger specific surface area and specific pore volume have stronger adsorption capacity.[25] So, during the sulfurization process, Gd_2O_3 grains in $(La_xGd_{1-x})_2O_3$ can easily combine to form larger oxysulfide particles, compared with $(La_{0.15}Gd_{0.85})_2O_3$.[26]

However, there was no obvious change in the specific surface area between $(La_{0.15}Gd_{0.85})_2O_3$, $(La_{0.3}Gd_{0.7})_2O_3$, $(La_{0.45}Gd_{0.55})_2O_3$, and $(La_{0.6}Gd_{0.4})_2O_3$. We attempt to attribute the increasing particle size to secondary crystallization.[27] It is commonly recognized that FE-SEM characterizes secondary particles, and smaller grains are more likely to combine through secondary crystallization. The smaller grains in the phosphors with similar crystalline size, i.e., Gd0.3, Gd0.45, and Gd0.6, preferentially contact with other grains to form larger secondary particles in order to decrease the surface energy of the particle system. Such

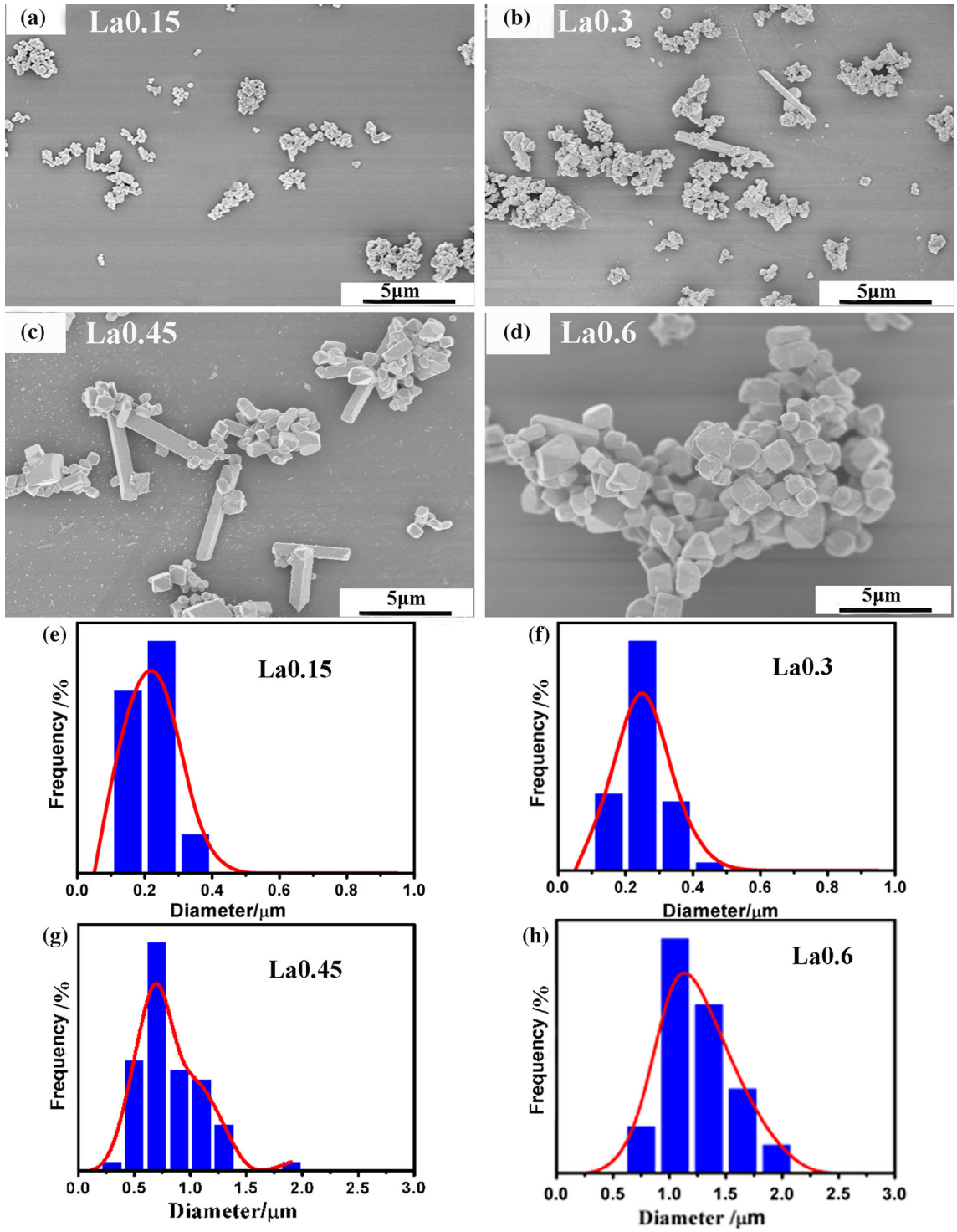

Fig. 6. FE-SEM images (a–d) and particle size distributions (e–h) of $(La_xGd_{1-x})_2O_2S$:Tb for x = 0.15, 0.30, 0.45, and 0.60, respectively.

interactions between particles will decrease in the molten liquid when they grow to a certain size. The presence of a small quantity of second-phase particles leads to growth of irregular particles,[28] thus the long strips observed in Fig. 6b and c are clearly due to excessive crystallization.

Dependence of Luminescence on La^{3+} Concentration

Figure 8 shows the luminescence properties of Gd-La:Tb excited at 254 nm, where the dominant emission corresponds to $^5D_4 \rightarrow {}^7F_J$ transition of Tb^{3+}. These characteristic peaks are found to split

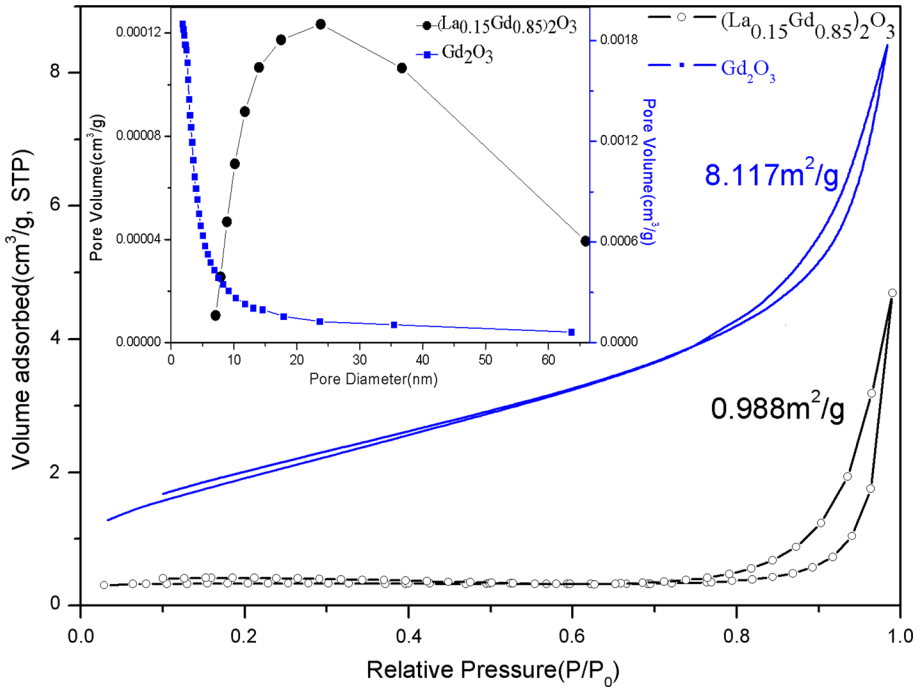

Fig. 7. Nitrogen adsorption–desorption isotherms and corresponding pore size distributions for Gd_2O_3 and $(La_{0.15}Gd_{0.85})_2O_3$ (inset).

Table II. Textual properties of mesoporous Gd_2O_3 and $(La_{0.15}Gd_{0.85})_2O_3$ powders

Sample	S_{BET} ($m^2\ g^{-1}$)	Pore size (nm)	Pore volume ($cm^3\ g^{-1}$)
Gd_2O_3	8.117	6.913	0.135
$(La_{0.15}Gd_{0.85})_2O_3$	0.988	27.738	0.007

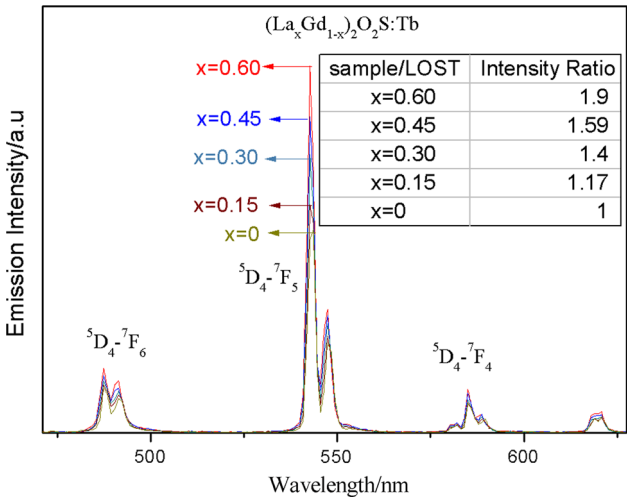

Fig. 8. Room-temperature emission spectra of Gd-La:Tb phosphor excited at 254 nm.

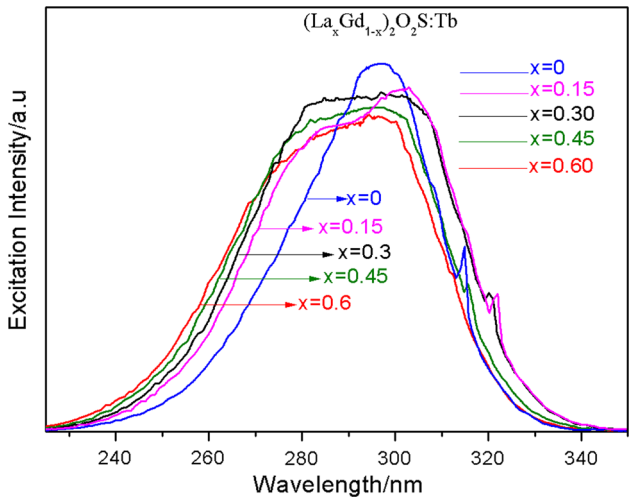

Fig. 9. Excitation spectra of Gd-La:Tb phosphors monitored at 544 nm.

into two peaks, originating from the lower crystal-field symmetry. As a non-Kramers ion, the electronic *J*-level degeneracy of Tb^{3+} can be destroyed by a low-symmetry crystal-field interaction, resulting in such splitting.[29] La^{3+} doping did not change these characteristic peaks of Tb^{3+}, but enhanced the luminescence intensity. The emission intensity at 544 nm increased monotonically as

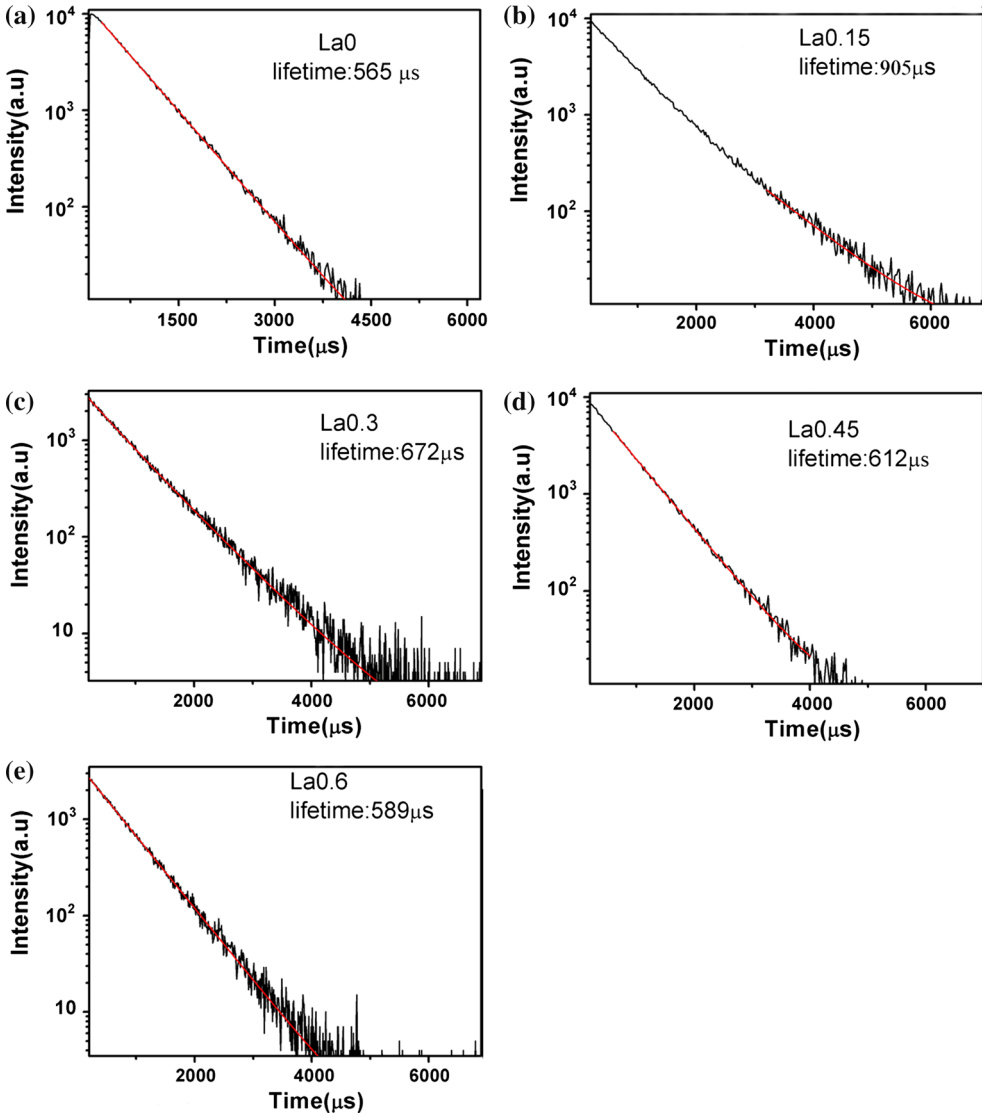

Fig. 10. Room-temperature luminescence decay curves for oxysulfide phosphors with different La^{3+} concentration: (a) Gd_2O_2S:Tb, (b) $(La_{0.15}Gd_{0.85})_2O_2S$:Tb, (c) $(La_{0.3}Gd_{0.7})_2O_2S$:Tb, (d) $(La_{45}Gd_{0.55})_2O_2S$:Tb, and (e) $(La_{0.6}Gd_{0.4})_2O_2S$:Tb. The decay curves were obtained by monitoring the Tb^{3+} emission at 544 nm under excitation at 254 nm.

Gd^{3+} was increasingly replaced by La^{3+}. The luminescence intensity of $(La_{0.4}Gd_{0.6})_2O_2S$:Tb reached 1.9 times that of GOST.

The excitation spectra of Gd-La:Tb from 200 nm to 400 nm when monitored at 544 nm are presented in Fig. 9. It is worth noting that addition of La^{3+} broadened the excitation band of the phosphors. Meanwhile, the bands shifted towards shorter wavelength with increasing La^{3+} content, enhancing the absorption intensity at 254 nm. Naturally, the higher emission intensity is caused by the intense absorption.

The position of the absorption band of the host material is influenced by the crystal field. Based on crystal-field theory, a stronger crystal field contributes to shorter-wavelength absorption for one Ln^{3+}.[30] Incorporation of La^{3+} ions induces greater distortion of the crystal structure and decreases the symmetry of the samples, influencing the crystal field.[31] Combining the DOS and EBS results shown in Fig. 4, the expansion of the conduction band width suggests extensibility of the atomic orbitals, which will intensify the crystal field.[32] Therefore, with increasing amounts of La^{3+} in Gd-La:Tb, the excitation spectrum shifted towards shorter wavelength due to the stronger crystal field.

Decay behavior is found to depend on the energy transfer, number of luminescent centers, defects, and impurities in the host material.[33] Bedekar attributed the different lifetimes found for Tb^{3+} ions to the surrounding environment.[34] Furthermore, a relatively longer PL decay time is related to a more symmetric site, whereas a shorter one is often associated with an asymmetric site.[35] Figure 10 shows the luminescence decay curves for Gd-La:Tb. All the normalized decay curves can be well fit using the single-exponential equation in Eq. 2:

$$I = I_0 \times \exp(-t/\tau), \quad (2)$$

where I represents the emission intensity at time t, I_0 is the emission intensity at $t = 0$, and τ is the decay lifetime. The fit lifetime for Gd-La:Tb was 565 μs, 905 μs, 672 μs, 612 μs, and 589 μs for La^{3+} concentration of 0 mol.%, 15 mol.%, 30 mol.%, 45 mol.%, and 60 mol.%, respectively. When 15 mol.% La^{3+} was incorporated into GOST, the appearance of defects led to longer lifetime, which sharply increased from 565 μs to 905 μs. However, the symmetry of the Tb^{3+} environment reduced with increasing La^{3+} concentration from 15 mol.% to 60 mol.%, with a gradual decrease in the $^5D_4$ lifetime, indicating a more asymmetric environment around Tb^{3+}. It is known that, the lower the symmetry of the lattice around the emitting ions, the higher the emission intensity,[36] which is consistent with the increasing luminescence intensity observed in Fig. 8.

CONCLUSIONS

$(La_xGd_{1-x})_2O_3$ materials were synthesized by the coprecipitation method and used to prepare Gd-La:Tb phosphors by the sulfide fusion method. Increasing the La^{3+} concentration in the Gd-La:Tb phosphor could increase the density of states of the conduction bands and narrow the energy gap. The enhanced electron density increased the repulsion and thereby decreased diffusion, decreasing the crystalline size. Compared with $(La_xGd_{1-x})_2O_3$, Gd_2O_3 with higher specific surface area and specific pore volume had stronger adsorption capacity, resulting in larger oxysulfide particles. The particle size of Gd-La:Tb increased as the La^{3+} concentration was increased from 15 mol.% to 60 mol.%.

As more Gd^{3+} was substituted by La^{3+}, the excitation spectrum shifted towards lower wavelength, and the luminescence intensity was enhanced on excitation at 254 nm. This was caused by a stronger crystal field. The decay behavior was related to the symmetry of the environment around Tb^{3+}. Lower symmetry with increasing La^{3+} concentration led to shorter lifetime.

ACKNOWLEDGEMENTS

The project is supported by the Priority Academic Program Development of Jiangsu Higher Education Institutions (PAPD) and National Natural Science Foundation of China (51202111).

ELECTRONIC SUPPLEMENTARY MATERIAL

The online version of this article (doi: 10.1007/s11664-017-5570-1) contains supplementary material, which is available to authorized users.

REFERENCES

1. C.Y. Liu, Y. Hou, and M.Y. Gao, *Adv. Mater.* 26, 6922 (2014).
2. Y.J. Ding, W.M. Yang, Q.T. Zhang, and L.X. Wang, *J. Mater. Sci-Mater. El.* 26, 1982 (2015).
3. F. Wang, B. Yang, J.C. Zhang, Y.N. Dai, and W.H. Ma, *J. Lumin.* 130, 473 (2010).
4. S. Chatterjee, V. Shanker, and H. Chander, *Mater. Chem. Phys.* 80, 719 (2003).
5. K. Li, Y. Zhang, X.J. Li, M.M. Shang, H.Z. Lian, and J. Lin, *Dalton. Trans.* 44, 4683 (2015).
6. R.N. Bhargava, V. Chhabra, B. Kulkarni, and J.V. Veliadis, *Phys. Stat. Sol (b).* 210, 621 (1998).
7. J. Liu, H.D. Luo, P.J. Liu, L.X. Han, X. Zheng, B. Xu, and X.B. Yu, *Dalton. Trans.* 41, 13984 (2012).
8. Z.G. Liu, X.D. Sun, S.K. Xu, J.B. Lian, X.D. Li, Z.M. Xiu, Q. Li, D. Huo, and J.G. Li, *J. Phys. Chem. C* 112, 2353 (2008).
9. P. Trtik and E.H. Lehmann, *Nucl. Instrum. Meth. A.* 788, 67 (2015).
10. J.X. Ma, M. Fang, and N.T. Lau, *J. Catal.* 158, 251 (1996).
11. G.A. Kumar, M. Pokhrel, and D.K. Sardar, *Mater. Lett.* 68, 395 (2012).
12. W. Wang, H.M. Kou, S.P. Liu, Y. Shi, J. Li, X.Q. Feng, Y.B. Pan, Y.S. Li, and J.K. Guo, *Ceram. Int.* 41, 2576 (2015).
13. K. Ohno and T, Abe, *J. Electrochem. Soc.* 141, 1252 (1994).
14. Y. Ding, J. Gu, J. Ke, Y.W. Zhang, and C.H. Yan, *Angew. Chem. Int. Ed.* 50, 12330 (2011).
15. F. Wang, Y. Han, C.S. Lim, Y.H. Lu, J. Wang, J. Xu, H.Y. Chen, C. Zhang, M.H. Hong, and X.G. Liu, *Nature* 463, 1061 (2010).
16. D.Q. Chen, Y.L. Yu, F. Huang, P. Huang, A.P. Yang, and Y.S. Wang, *J. Am. Chem. Soc.* 132, 9976 (2010).
17. E.M. Chan, G. Han, J.D. Goldberg, D.J. Gargas, A.D. Ostrowski, P.J. Schuck, B.E. Cohen, and D.J. Milliron, *Nano Lett.* 12, 3839 (2012).
18. L. Hernández-Adame, A. Méndez-Blas, J. Ruiz-García, J.R. Vega-Acosta, F.J. Medellín-Rodríguez, and G. Palestino, *Chem. Eng. J.* 258, 136 (2014).
19. U. Holzwarth and N. Gibson, *Nat. Nanotechnol.* 6, 534 (2011).
20. X. Yan, G.R. Fern, R. Withnall, and J. Silver, *Nanoscale* 5, 8640 (2013).
21. R. Vijayakumar, G. Venkataiah, and K. Marimuthu, *J. Alloys Compd.* 652, 234 (2015).
22. Y. Li, X.T. Wei, H.M. Chen, G. Pang, Y. Pan, L. Gong, L.L. Zhu, G.Y. Zhu, and Y.X. Ji, *J. Lumin.* 168, 124 (2015).
23. R. Vali, *Comp. Mater. Sci.* 37, 300 (2006).
24. J.B. Lian, X.D. Sun, J.G. Li, B. Xiao, and K. Duan, *Mater. Chem. Phys.* 122, 354 (2010).
25. A. Vinu, C. Streb, V. Murugesan, and M. Hartmann, *J. Phys. Chem. B* 107, 8297 (2003).
26. Y.J. Ding, P.D. Han, L.X. Wang, and Q.T. Zhang, *Rare Met.* (2015). doi:10.1007/s12598-015-0577-3.
27. S.H. Xuan, Y.X.J. Wang, J.C. Yu, and K.C.F. Leung, *Chem. Mater.* 21, 5079 (2009).
28. J.J. Li, J.C. Wang, and G.C. Yang, *Rare. Metal. Mater. Eng.* 37, 1746 (2008).
29. F. Zhao, M. Yuan, W. Zhang, and S. Gao, *J. Am. Chem. Soc.* 128, 11758 (2006).
30. Y.Y. Li, *Nonferrous Met.* 63, 122 (2011).
31. G.Q. Chen, F.L. Wang, W.C. Ji, Y.X. Liu, and X. Zhang, *Superlattice. Microstruct.* 90, 30 (2016).
32. L. Chen, X.L. Chen, F.Y. Liu, H.H. Chen, H. Wang, E.L. Zhao, Y. Jiang, T.S. Chan, C.H. Wang, W.H. Zhang, Y. Wang, and S.F. Chen, *Sci. Rep. UK* 5, 11514 (2015).
33. G. Jia, Y. Song, M. Yang, Y. Huang, L. Zhang, and H. You, *Opt. Mater.* 31, 1032 (2009).
34. V. Bedekar, D.P. Dutta, M. Mohapatra, S.V. Godbole, R. Ghildiyal, and A.K. Tyagi, *Nanotechnology* 20, 125707 (2009).
35. S.K. Gupta, P.S. Ghosh, A.K. Yadav, N. Pathak, A. Arya, S.N. Jha, D.B. Bhattacharyya, and R.M. Kadam, *Inorg. Chem.* 55, 1728 (2016).
36. H.X. Mai, Y.W. Zhang, R. Si, Z.G. Yan, L.D. Sun, L.P. You, and C.H. Yan, *J. Am. Chem. Soc.* 128, 6426 (2006).